

Journal of Materials Chemistry A

Materials for energy and sustainability

Accepted Manuscript

This article can be cited before page numbers have been issued, to do this please use: Z. Cao, V. E. Gonzalez, D. Minh, X. Zhang, Y. Wang, K. Khawaja, J. J. Kjeldahl, A. Berzansky, L. Whittaker-Brooks, F. Yan, J. M. Luther and H. Wang, *J. Mater. Chem. A*, 2026, DOI: 10.1039/D6TA01022A.



This is an Accepted Manuscript, which has been through the Royal Society of Chemistry peer review process and has been accepted for publication.

Accepted Manuscripts are published online shortly after acceptance, before technical editing, formatting and proof reading. Using this free service, authors can make their results available to the community, in citable form, before we publish the edited article. We will replace this Accepted Manuscript with the edited and formatted Advance Article as soon as it is available.

You can find more information about Accepted Manuscripts in the [Information for Authors](#).

Please note that technical editing may introduce minor changes to the text and/or graphics, which may alter content. The journal's standard [Terms & Conditions](#) and the [Ethical guidelines](#) still apply. In no event shall the Royal Society of Chemistry be held responsible for any errors or omissions in this Accepted Manuscript or any consequences arising from the use of any information it contains.

Chloride Modification of Vacuum-Assisted Blade-Coated Perovskite Solar Cells and Mini-Modules in Ambient Environment

Zikun Cao,^{1†} Violeta Elora Gonzalez,^{1†} Duong Nguyen Minh,² Xinwen Zhang,² Yizhao Wang,³ Kausar Khawaja,³ Jacob Kjeldahl Jensen,⁴ Alex Berzansky,⁴ Luisa Whittaker-Brooks,⁴ Feng Yan,³ Joseph M. Luther,² He Wang^{1,*}

¹ Department of Physics, University of Miami, Coral Gables, FL 33146, USA

² National Laboratory of the Rockies, Golden, CO 80401, USA

³ Materials Science and Engineering Program, School for Engineering of Matter, Transport and Energy, Arizona State University, Tempe, AZ 85287, USA

⁴ Department of Chemistry, University of Utah, Salt Lake City, Utah 84112, USA

Email: hewang@miami.edu

† These authors contributed equally to this work.

Abstract

Scalable deposition of perovskite thin films under ambient conditions remains a key challenge for the commercialization of perovskite photovoltaics, primarily due to the difficulty of controlling crystallization kinetics and suppressing non-radiative recombination during film formation. In this work, we present an effective strategy to modulate crystallization kinetics and non-radiative recombination in vacuum-quenched blade-coated perovskite films processed in air using chloride-based additives. By systematically comparing PbCl_2 and 3-



chloropropylamine hydrochloride (Cl-PACl), we elucidate how different chloride incorporation pathways influence crystallization behavior and optoelectronic properties. In-situ transmission and in-situ photoluminescence measurements reveal that PbCl_2 acts as a transient additive that slows intermediate/perovskite phase formation while suppressing non-radiative recombination, leading to improved film quality. In contrast, Cl-PACl introduces additional trap states that deteriorate optoelectronic performance. As a result, PbCl_2 -modified perovskite solar cells achieve a champion power conversion efficiency (PCE) of 24.2% and remarkable operational stability, retaining over 90% of their initial performance after 800 hours of continuous illumination. Furthermore, we successfully scaled the process, fabricating a perovskite mini-module that delivered a champion efficiency of 18.0%. This study underscores the critical importance of coupling vacuum-assisted blade coating with transient additive engineering for achieving high-performance, stable, and scalable perovskite photovoltaics processed in ambient air.

Keywords: Chloride; Perovskite Solar Cells; Blade coating; Vacuum quenching; Crystallization; Ambient environment.

View Article Online

DOI: 10.1039/C5TA01022A



1. Introduction

Metal halide perovskite solar cells (PSCs) have attracted tremendous attention as a promising next-generation photovoltaic technology, owing to their exceptional optoelectronic properties such as a tunable bandgap, a high absorption coefficient, long carrier diffusion lengths, and high defect tolerance. In the past decade, the certified power conversion efficiency (PCE) of PSCs has surged from below 4% to 27%,¹ rivaling that of crystalline silicon solar cells. However, most high-performance devices are still fabricated using spin coating combined with antisolvent quenching in an inert glovebox environment. This method enables extremely rapid solvent extraction, triggering fast and uniform nucleation and crystallization, which is highly effective at the lab scale. Yet, its inherent limitations in scalability and compatibility with industrial manufacturing hinder the commercial prospects of perovskite photovoltaics.²⁻⁵

To bridge the gap between laboratory-scale fabrication and scalable manufacturing, various solution-based deposition techniques have been explored for perovskite photovoltaics. Spin coating, while highly effective for achieving high-efficiency devices at the laboratory scale, is inherently limited to small-area substrates and typically relies on antisolvent quenching to induce rapid and uniform crystallization, which is difficult to translate to scalable processing. In contrast, fully scalable techniques such as slot-die coating are well suited for large-area, continuous production, but typically require a larger volume of precursor solution, particularly due to system dead volume and continuous fluid delivery.⁶ Blade coating occupies an intermediate and strategically important position between these two approaches, enabling controlled deposition over mid-area substrates with relatively low material consumption. As such, blade coating serves as a practical bridge between spin coating and slot-die coating, allowing processing strategies developed at the laboratory scale to be systematically adapted toward scalable manufacturing.⁷⁻¹¹ However, unlike spin coating, blade coating cannot readily employ antisolvent quenching, and the solvent removal dynamics are intrinsically slower, particularly under ambient conditions, where moisture and oxygen can further complicate crystallization behavior and film formation.¹²⁻¹⁴ Alternative quenching strategies, such as vacuum-assisted quenching, have therefore been developed for blade-coated perovskite films.



Nevertheless, the quenching speed of vacuum-assisted processes is typically much slower than that of antisolvent methods, making precise control over nucleation and crystallization kinetics a central challenge.¹⁵⁻¹⁸

The key to obtaining high-quality perovskite films under such conditions, therefore, lies in actively regulating the nucleation and crystallization kinetics to compensate for the slower quenching speed. Since vacuum quenching alone may be insufficient to drive optimal nucleation, the crystallization process must be tuned through other means. Specifically, slowing down the crystallization rate becomes crucial, as it allows for better structural reorganization and growth of compact but larger grains, mitigating the issues caused by insufficiently rapid nucleation. Common strategies to slow down crystallization include processing at lower temperatures¹⁹⁻²⁰ and employing additive engineering.²¹⁻²⁴

Among various additives, chloride-based compounds have proven to be one of the most effective in modulating crystallization kinetics for spin coating. Notably, methylammonium chloride (MACl) is widely recognized as one of the most effective chloride additives for significantly enhancing crystallization quality and rate.²⁵⁻²⁷ However, not all chlorides facilitate crystallization as rapidly as MACl. The different chemical properties and incorporation mechanisms of chloride additives can lead to varied crystallization dynamics.²⁸⁻³² Understanding these slower-acting chlorides is crucial for selecting the appropriate additive to match specific processing conditions, such as the modest quenching speed of vacuum-assisted blade coating.

In this work, we systematically investigate the influence of chloride additives with distinct incorporation mechanisms under ambient vacuum-assisted blade-coating conditions. Our study focuses primarily on a comparative analysis between PbCl_2 , which introduces Cl^- at the X-site and Pb^{2+} at the B-site, and 3-chloropropylamine hydrochloride (Cl-PACl),³²⁻³³ which provides simultaneous modification at both the A-site (via the chloropropylamine cation, Cl-PA^+) and the X-site (via Cl^-) in the 3D ABX_3 perovskite lattice. We demonstrate that these different additives profoundly tune the crystallization kinetics and non-radiative recombination—factors



that are directly correlated with the resulting device performance and operational stability. This comparison allows us to elucidate how different additive incorporation pathways regulate crystallization behavior, defect formation, and ultimately the photovoltaic performance.

Through this additive engineering approach, we achieved high-efficiency PSCs with a champion PCE of 24.2% using dual modification of MAI and PbCl_2 . Furthermore, by extending the same scalable blade-coating process to larger areas, we successfully fabricated perovskite mini-modules that delivered a champion efficiency of 18.0%. These results demonstrate a viable and promising route toward the ambient, large-area, and cost-effective manufacturing of perovskite photovoltaics, bridging the gap between laboratory research and industrial production.

2. Results and Discussion

2.1 Role of MAI in the Crystallization and Performance of Blade-Coated Perovskite Solar Cells

We investigated the fabrication of $\text{FA}_{0.92}\text{Cs}_{0.08}\text{PbI}_3$ perovskite films in ambient air using a blade-coating process followed by immediate vacuum quenching. A schematic of this process is illustrated in **Figure 1a**. The quenching kinetics of our vacuum chamber, detailed in **Figure S1**, show a rapid pressure drop from 1 atm (1013 mbar) to 0.076 mbar within 10 seconds, reaching 0.021 mbar by 20 seconds, facilitating fast solvent removal. All vacuum-assisted blade-coating processes in this study were conducted under ambient conditions with a relative humidity of approximately 45–55% RH and room temperature at 20 °C.

The introduction of MAI as an additive profoundly influenced the crystallization pathway. For the precursor without MAI, the film after vacuum quenching appeared light yellow (**Figure 1b1**). Subsequent exposure to ambient air (45–55% RH) induced only a slight darkening (**Figure 1b2**), with the characteristic dark brown/black color of perovskite emerging only after final thermal annealing (**Figure 1b3**). In contrast, the precursor with 10% MAI exhibited markedly different behavior. While the post-quenching film appeared a slightly darker yellow (**Figure 1c1**), exposure to ambient humidity triggered an instantaneous and



pronounced darkening to a very dark brown (**Figure 1c2**). This stark visual contrast highlights a critical interaction between moisture and MACl, where the humidity is known to accelerate the penetration of MACl through the film thickness, promoting a more uniform and rapid crystallization of the perovskite phase prior to annealing.³⁴

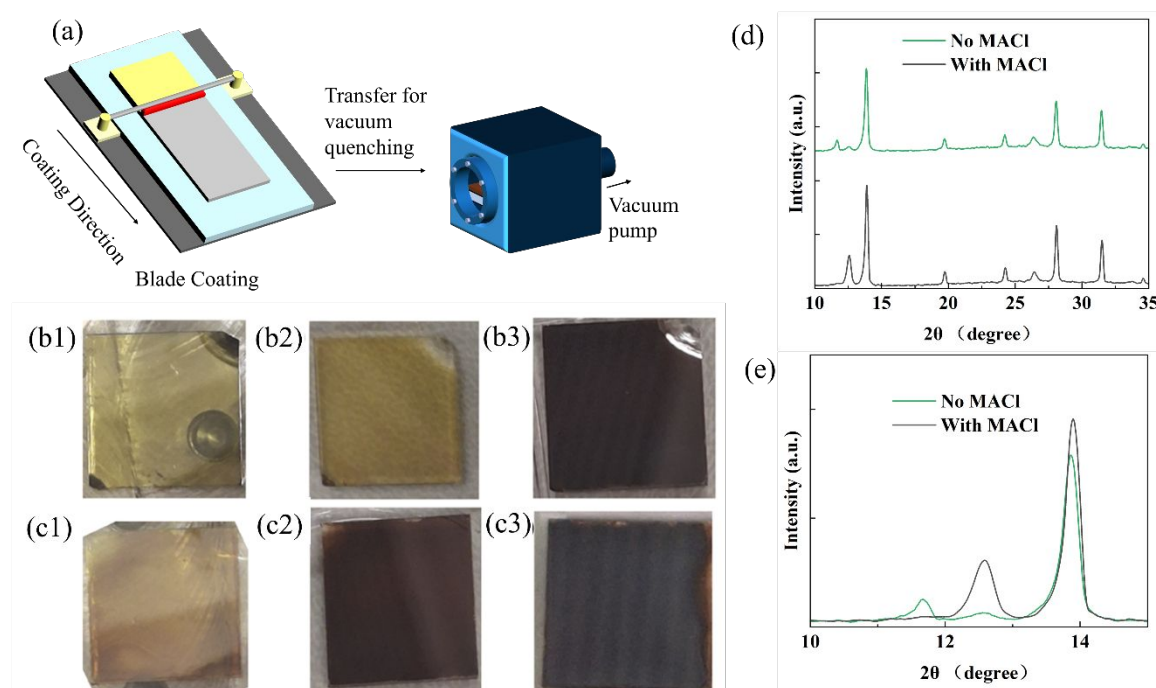


Figure 1. Blade-coating process and the role of MACl in perovskite crystallization. (a) Schematic illustration of the blade-coating and vacuum quenching setup. (b-c) Photographs of blade-coated $\text{FA}_{0.92}\text{Cs}_{0.08}\text{PbI}_3$ films on $2\text{ cm} \times 2\text{ cm}$ substrates: (b1-b3) without MACl, and (c1-c3) with 10% MACl additive, captured at key stages - after vacuum quenching (b1, c1; photos taken with samples inside vacuum chamber), after exposure to ambient air (b2, c2), and after thermal annealing (b3, c3). (d) Full-range and (e) zoomed-in XRD patterns of blade-coated perovskite thin films w/o MACl.

The enhanced crystallization induced by MACl was confirmed through structural analysis. X-ray diffraction (XRD) patterns (**Figure 1d, 1e**) revealed that the film with 10% MACl exhibited significantly stronger peaks at 13.93° , 28.10° , and 31.57° (associated with the (110), (220), and (310) perovskite planes, respectively) and a reduced peak at 12.63° (from unreacted PbI_2)³⁵⁻³⁶ compared to the control film. This indicates superior crystallinity and more complete precursor conversion.



Consequently, the MAI-*incorporated* film demonstrated stronger absorption (**Figure 2a**) and a more intense, slightly red-shifted steady-state photoluminescence (PL) emission (**Figure 2b**), consistent with improved material quality and reduced defect density. Time-resolved photoluminescence (TRPL) decay curves (**Figure 2c**) were fitted using a bi-exponential model, with the detailed fitting parameters summarized in Supporting Information (SI) **Table S1**. Based on the calculated average carrier lifetimes using an amplitude-weighted expression, the MAI-treated film exhibits a significantly prolonged lifetime of 173.1 ns compared to 66.3 ns for the control sample, indicating substantially suppressed non-radiative recombination. Morphological inspection via scanning electron microscopy (SEM) showed that the MAI-treated film (**Figure 2e**) possessed larger, more uniform grains with an average size of 400 nm, a substantial increase over the 130 nm grains in the control film (**Figure 2d**). This microstructural improvement directly correlated with enhanced charge carrier properties.

This collective enhancement in material properties culminated in superior photovoltaic device performance. After optimizing the MAI concentration (data for 5%, 10%, and 15% provided in **Figure S2a**), 10% was identified as optimal for this composition. The current density-voltage (J-V) characteristics of champion devices (**Figure 2f**) demonstrate a dramatic improvement with MAI addition. The control device (no MAI) achieved a short-circuit current density (J_{sc}) of 19.5 mA/cm², an open-circuit voltage (V_{oc}) of 1.04 V, a fill factor (FF) of 0.74, and a PCE of 15.0%. The device with 10% MAI showed significantly enhanced performance, with a J_{sc} of 24.8 mA/cm², a V_{oc} of 1.07 V, an FF of 0.75, and a champion PCE of 19.8%. This comprehensive performance boost, mainly an increase in J_{sc} , is directly attributable to the MAI-induced improvements in crystallinity and grain size.



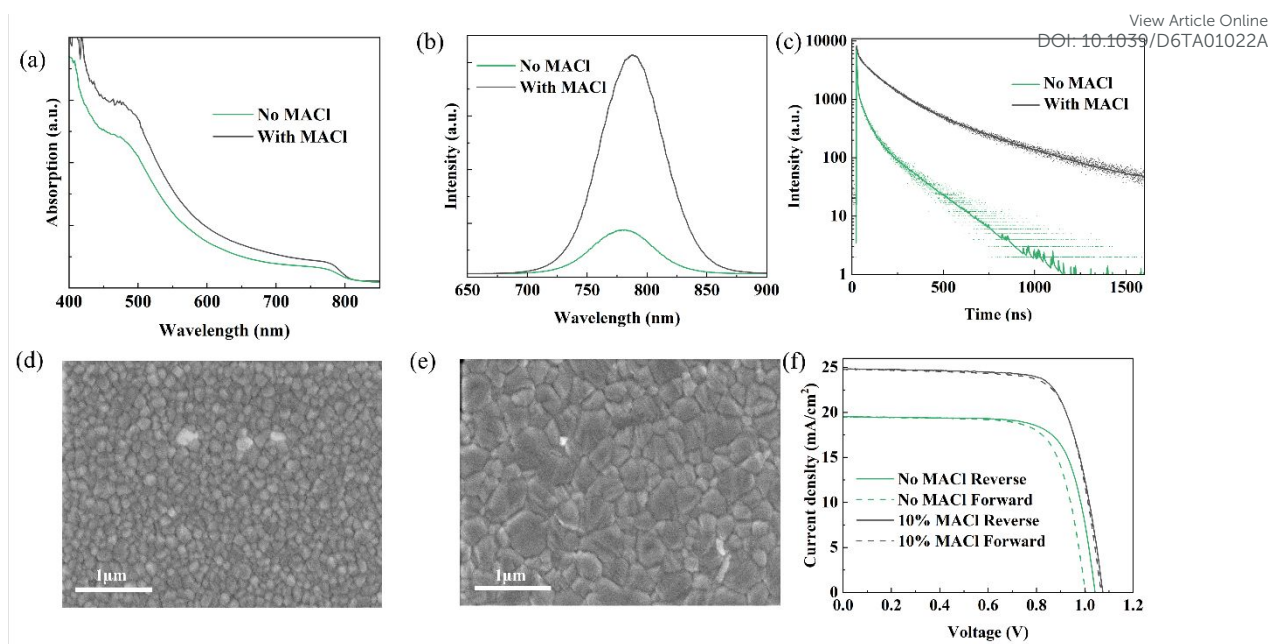


Figure 2. Effect of MACl on the structural, optical, and morphological properties of blade-coated perovskites. (a) UV-Visible spectrum of blade-coated perovskite thin films w/o MACl. (b) Steady-state PL spectra. (c) TRPL decay curves (dot: experimental data; solid line: fit). SEM images of the films (d) without 10% MACl and (e) with MACl additive. (f) J-V characteristics of the corresponding PSCs.

2.2 Comparative Impact of Chlorinated Additives on Crystallization and Film Quality

Although the film exhibits decent crystallinity, a previous study reported the formation of voids at the buried perovskite interface, particularly under conditions of rapid crystallization or phase evolution, which has been attributed to volume shrinkage during film formation or subsequent processing.³⁷ While MACl effectively accelerates crystallization, we further explored additional chlorinated additives that enable more moderate regulation of crystallization kinetics, better matched to the intrinsically slow solvent extraction associated with vacuum-assisted quenching. Specifically, we selected PbCl_2 and Cl-PACl, which tend to slow down nucleation and crystal growth compared to MACl. The composition with different amounts of PbCl_2 or Cl-PACl are shown in **Figure S2b** and **S2c**. Based on device optimization, the performance shows a trend of initially increasing and then decreasing with increasing additive concentration. At low concentrations, the additives are insufficient to effectively



regulate crystallization kinetics. At optimal concentrations (2% PbCl_2 and 5% Cl-PACl), improved crystallinity and reduced defect density lead to enhanced device performance. However, further increasing the additive concentration introduces adverse effects, such as structural disorder or impeded charge transport, resulting in performance degradation. Therefore, 2% PbCl_2 and 5% Cl-PACl incorporated into the baseline $\text{FA}_{0.92}\text{Cs}_{0.08}\text{PbI}_3$ precursor with 10% MACl were selected as the optimal concentrations to form the treatment groups.

In-situ experiments are highly effective for probing dynamic nucleation and crystallization processes,³⁸⁻³⁹ particularly the formation of intermediate phases consisting of a mixture of perovskite and precursor-derived species. In this work, we performed in-situ optical measurements using custom-built equipment, including in-situ transmission and in-situ PL, to directly monitor the evolution of optical properties during vacuum quenching, where the precursor transforms from a liquid phase into intermediate and eventually perovskite phases. For the in-situ transmission measurements (analogous to absorption measurements but monitoring transmitted light), we tracked the transmission of white light through the films (**Figure S3**). A white light source, with maximum intensity at a wavelength of 611 nm, was directed from the top of the vacuum chamber through a glass window, while the transmitted light was collected from the bottom through another glass window using an optical fiber coupled to a visible spectrometer. A decrease in transmitted intensity corresponds to increased formation of the perovskite and/or intermediate phase. Here, the transmitted intensity is normalized to its initial value at 611 nm (**Figure 3a**). The transmission decreases most rapidly in the pristine sample, whereas it decreases significantly more slowly in the PbCl_2 -modified sample, indicating a delayed formation of the perovskite and/or intermediate phase.

Additionally, in-situ PL measurements were conducted using a charge-coupled device (CCD) camera that collects emission spectra with a 1-second integration time every 2 seconds. **Figures 3b–d** show the evolution of PL during vacuum quenching, tracking the transition from liquid precursor to intermediate phase for pristine (MACl -only), Cl-PACl -modified, and PbCl_2 -modified perovskite samples. **Figure 3e** summarizes the maximum PL intensity as a

function of time for all three samples. The PbCl_2 -modified sample exhibits the highest PL intensity, which is attributed to reduced non-radiative recombination and thus improved film quality. Overall, these results provide direct experimental evidence that PbCl_2 not only slows the formation of the perovskite and/or intermediate phase, but also suppresses non-radiative recombination.

The structural impact of final films with these additives was probed by XRD (**Figure 3f**). All samples exhibited the characteristic (110), (220), and (310) peaks of the perovskite α -phase, confirming successful formation of the desired structure. However, distinct differences were observed in secondary phases. A peak at 12.63° , indicative of excess PbI_2 , was prominent in the pristine (MAcI only) and Cl-PACl modified samples, accompanied by a decrease in the intensity of the main (110) perovskite peak. In contrast, the PbCl_2 -modified sample showed a very weak PbI_2 signal, suggesting a more complete conversion of precursors into the perovskite phase.

Morphological analysis via SEM (**Figure 3g-3i**) provided further insight. The PbCl_2 -modified film displayed the largest grain size averaging ~ 500 nm (**Figure 3i**), even exceeding the pristine (MAcI-only) sample averaging ~ 280 nm (**Figure 3g**). This suggests that the moderate slowing of crystallization induced by PbCl_2 is beneficial, allowing for more extensive grain growth. After surface passivation of the PbCl_2 -modified perovskite film using phenethylammonium iodide (PEAI), the surface morphology remains compact and uniform, as shown in **Figure S4**. No noticeable changes in grain size or film continuity are observed. Although Cl-PACl also slows crystallization (resulting in larger grain size average ~ 400 nm, larger than the pristine sample), its large molecular size hinders effective integration into the crystal lattice. This results in unreacted PbI_2 (as depicted in the XRD profile in **Figure 3f**) and the formation of bright spots in the SEM image (**Figure 3h**), likely associated with Pb-rich regions or phase impurities. This indicates that an effective additive must not only modulate crystallization kinetics but also interact favorably with the precursor solvents and the evolving Pb-I crystal framework.



To investigate whether Cl^- of PbCl_2 remains in the final film, we performed both EDS (Figure S5) and XPS (Figure S6) measurements to quantify the residual chlorine content. The results show that the chlorine content in the final films is very low for all samples, indicating that most of the chloride species do not remain in the perovskite lattice after film formation and annealing. This suggests that Cl^- of PbCl_2 primarily acts as a transient additive during the crystallization process, influencing intermediate phases and regulating crystallization kinetics, rather than being incorporated into the final perovskite structure.

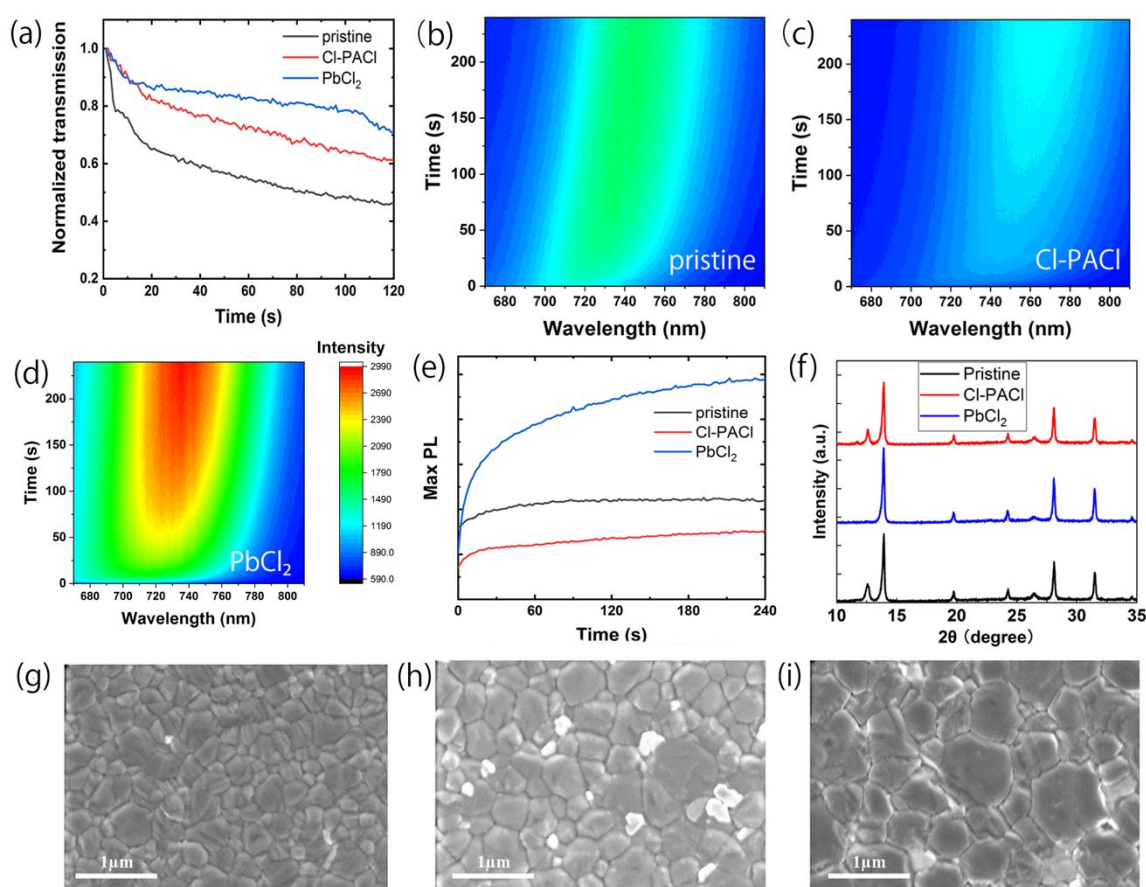


Figure 3. Comparative analysis of PbCl_2 and Cl-PACl additives on blade-coated perovskite films. (a) In-situ transmission of white light through the films during vacuum quenching from the liquid precursor to the intermediate phase. (b–d) In-situ PL evolution of perovskite films during vacuum quenching for (b) pristine (MACl only), (c) Cl-PACl-, and (d) PbCl_2 -modified perovskites. Color bar is kept the same for panels b-d to facilitate comparison. (e) Maximum PL intensity as a function of time for the three films, extracted from panels (b–



d). (f) XRD patterns of the corresponding films. (g–i) SEM images of the films: (g) pristine (MAcI only), (h) Cl-PACl-modified, and (i) PbCl₂-modified.

View Article Online
DOI: 10.1039/C6TA01022A

To evaluate the resulting optoelectronic quality, we performed steady-state and TRPL spectroscopy. The steady-state PL spectra (**Figure 4a**) showed a peak at 780 nm for all samples, again confirming the unchanged bandgap. The PbCl₂ film exhibited a significant increase in PL intensity, while the Cl-PACl film showed a pronounced decrease. This trend was corroborated by TRPL (**Figure 4b**). Bi-exponential fitting (**Table S1**) yielded an amplitude-weighted charge carrier lifetime of 246.2 ns for the PbCl₂ sample, significantly longer than the 173.1 ns of the pristine sample and the 110.2 ns of the Cl-PACl sample. The enhanced PL intensity and prolonged lifetime for the PbCl₂ sample indicate effective suppression of non-radiative recombination pathways.⁴⁰ Conversely, the rapid decay and quenched emission from the Cl-PACl sample point to increased trap-assisted recombination, consistent with the structural defects identified by XRD.

Further investigation into charge carrier dynamics was conducted using transient absorption spectroscopy (TAS). The ground state bleaching (GSB) signal, centered around 784 nm, was monitored for PbCl₂-modified perovskite (**Figure 4c**). The TAS of pristine and Cl-PACl modified samples were shown in **Figure S7**. The decay kinetics at this wavelength were fitted with a triple-exponential function (**Figure 4d**). The fitting parameters are shown in **Table S2**. The component with a negative amplitude (A_1) is associated with hot-carrier relaxation. The longer-lived component is associated with bimolecular (radiative) recombination, while the short-lived component is linked to trap-assisted recombination.^{41–42} The average lifetime can be extracted from the amplitude and its associated lifetime. The average lifetimes for three samples are 9.1 ns for pristine film, 5.2 ns for Cl-PACl modified film, and 11.4 ns for PbCl₂ modified film. The dominance of the long-lived component in the PbCl₂ sample signifies a lower density of traps and more efficient charge carrier diffusion. The Cl-PACl sample shows an exceptionally fast short decay lifetime (0.36 ns), revealing a high rate of non-radiative recombination from deep trap states. These TAS results are fully consistent with the PL and



TRPL data, conclusively demonstrating that PbCl_2 effectively passivates bulk defects, whereas Cl-PACl introduces deleterious trap states that degrade optoelectronic performance.

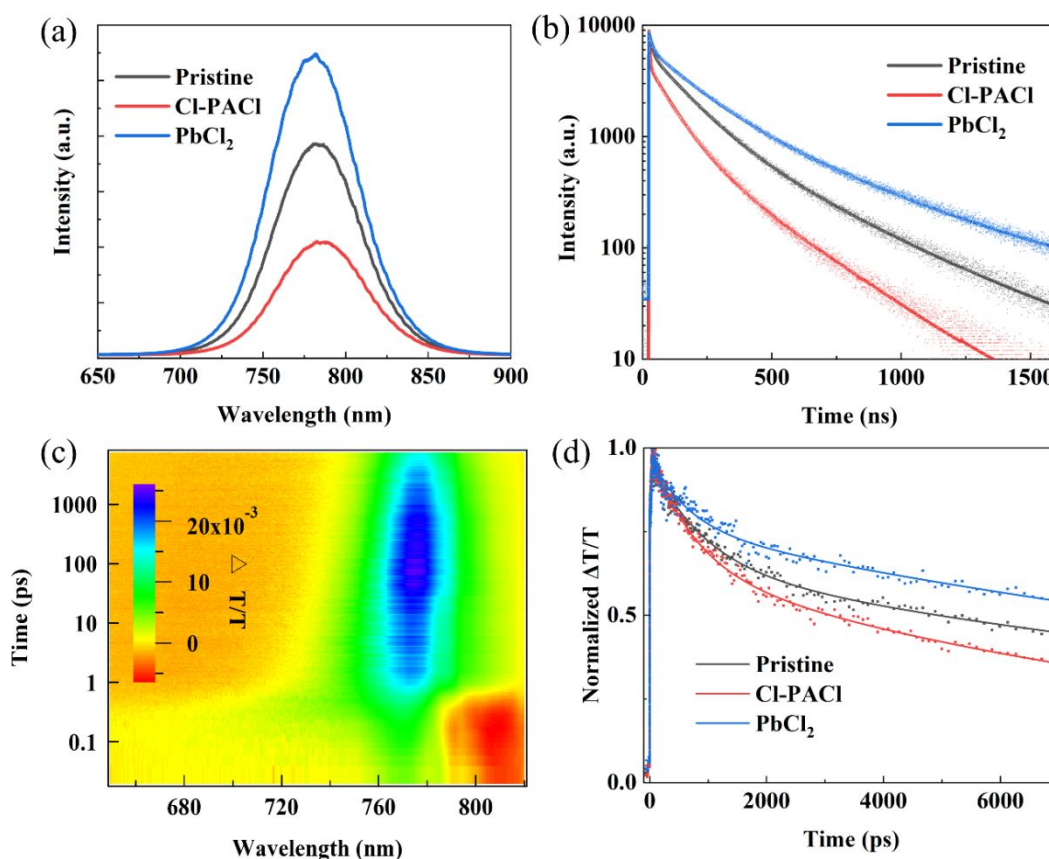


Figure 4. Charge carrier dynamics of blade-coated perovskite films with different additives. (a) Steady-state PL and (b) TRPL (dot: experimental data; solid line: fit) for the pristine (MAcI only), Cl-PACl-modified, and PbCl_2 -modified films. (c) Representative transient absorption spectra map for the PbCl_2 -modified sample, showing GSB features. (d) Normalized kinetics extracted from the transient absorption spectra at the GSB maximum for all three samples (dot: experimental data; solid line: fit).

2.3. Device Performance and Scalability to Mini-Modules

The superior structural and optoelectronic properties of the PbCl_2 -modified films directly translated to enhanced photovoltaic performance. Solar cells with an FTO/Me-4PACz+Perovskite/PEAI/PCBM/BCP/Cu architecture were fabricated to evaluate the efficacy of the different additives. In all films and devices, Me-4PACz was introduced via co-deposition with the perovskite precursor, forming a self-assembled interfacial layer at the substrate during



film formation. Since Me-4PACz was incorporated uniformly in all samples, its influence is consistent across all conditions and does not affect the comparative analysis of different chloride additives. The J-V characteristics are summarized in **Figure 5a**. Consistent with the film analysis, the PbCl₂-based devices showed a comprehensive improvement in all photovoltaic parameters, achieving a champion PCE of 24.2% (Voc=1.14 V, Jsc=25.8 mA/cm², FF=0.82). This is attributed to the synergistic effects of enhanced crystallinity, larger grain size, and suppressed non-radiative recombination, which collectively boost charge generation and extraction. In contrast, devices incorporating Cl-PACl exhibited a compromised performance. A slight increase in FF suggested some degree of passivation, but this was overwhelmingly negated by a significant reduction in Jsc (Jsc=22.8 mA/cm², FF=0.77, Voc=1.07V, PCE=18.8%), a direct consequence of the poor film quality. For comparison, devices fabricated with phenethylammonium chloride (PEACl) also exhibit a reduced Jsc (**Figure S1d**), similar to the Cl-PACl-modified devices. This behavior is attributed to the incorporation of oversized organic cations at the A-site, which hinders efficient charge transport and carrier collection. The cross-sectional SEM show that the three film thicknesses are similar (**Figure S8**), with a thickness of ~500 nm. This indicates that the observed differences in device performance are not related to variations in film thickness.

Statistical analysis of over 20 devices for each group (**Figure S9**) confirmed these trends. The average PCE, Jsc, Voc, and FF of PbCl₂-modified PSCs were 22.5% ± 0.6%, 25.6 ± 0.4 mA/cm², 1.10 ± 0.02 V, 0.80 ± 0.01. The average PCE, Jsc, Voc, and FF of Cl-PACl-modified PSCs were 18.1% ± 0.9%, 22.1 ± 0.8 mA/cm², 1.05 ± 0.01 V, 0.76 ± 0.02, while the pristine devices exhibited average PCE, Jsc, Voc, and FF of 18.9% ± 0.9%, 24.2 ± 0.7 mA/cm², 1.05 ± 0.02 V, 0.71 ± 0.02. Furthermore, the PbCl₂ devices demonstrated a narrower performance distribution, highlighting their superior reproducibility and fabrication robustness.

The operational stability of encapsulated devices was assessed under continuous 1-sun illumination at ~65 °C (**Figure 5b**). The J-V scans were conducted every two hours. The initial efficiencies for the three cases in the stability test are 18.9%, 17.8% and 22.0% for pristine device, Cl-PACl-modified device, and PbCl₂-modified device. The PbCl₂-modified devices



exhibited exceptional durability, retaining over 90% of their initial PCE after 800 hours. The pristine and Cl-PACl modified devices, however, began to degrade significantly after only 300 and 200 hours, respectively. This accelerated failure aligns with the higher intrinsic defect densities and structural instabilities in these films, which are exacerbated under thermal and light stress. We have further performed (i) thermal stability tests at 65 °C in a glovebox using unencapsulated devices, and (ii) humidity stability tests at 85% RH at room temperature using encapsulated devices. (**Figure S12**) The results show that the PbCl₂-modified devices exhibit improved stability compared to the control samples under both thermal and high-humidity conditions, with a more pronounced improvement observed under thermal stress. Under high-humidity conditions, the stability of encapsulated devices is strongly influenced by the effectiveness of the encapsulation layer, which limits direct moisture ingress. Therefore, the intrinsic differences between the perovskite films are less pronounced in this test configuration, particularly for small-area devices.

To demonstrate the scalability of this optimized formulation, perovskite solar mini-modules were fabricated using the PbCl₂-based ink. The module structure was identical to the single cells but incorporated laser scribing to create series-connected sub-cells. The detailed laser patterning procedures (P1–P4) and optimization of parameters are detailed in the SI experimental section and **Figure S10**.^{19, 43–45} The 6-cell mini-module with a total aperture area (including dead area) of 12.24 cm² achieved a champion PCE of 18.0 %, with an Voc of 6.92 V, a Jsc of 22.97 mA/cm², and a FF of 68% (**Figure 5c**). In addition, five independently fabricated modules exhibited PCEs ranging from 16.6% to 18.0%, with an average efficiency of 17.1 ± 0.6%, demonstrating good reproducibility of the scalable fabrication process (**Figure S11**). This successful upscaling confirms the practical potential of the PbCl₂ additive for the fabrication of efficient and reliable larger-area perovskite photovoltaics.



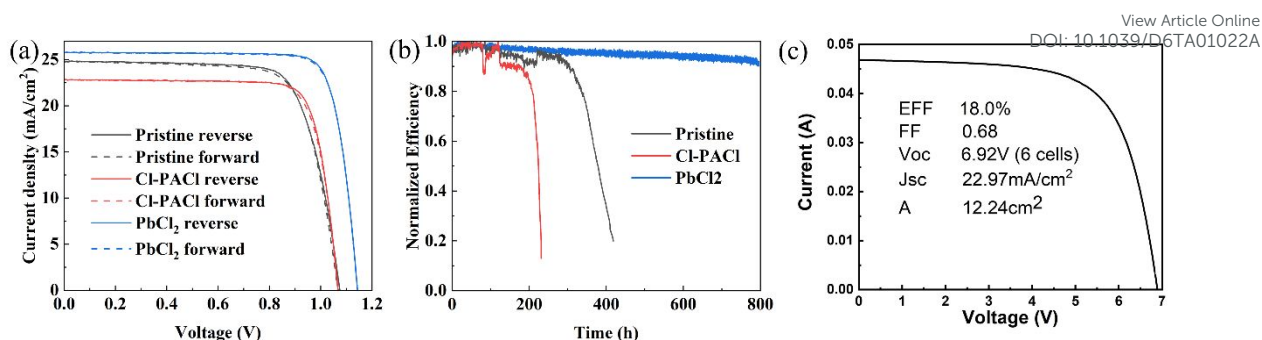


Figure 5. Device performance, stability, and module integration. (a) J-V curves of champion solar cells based on pristine (MAcI only), Cl-PACl-modified, and PbCl₂-modified perovskite films. (b) Operational stability of encapsulated devices under continuous 1-sun illumination at 65 °C, presented as normalized PCE over time. (c) J-V characteristic of a series-interconnected mini-module fabricated using the optimized PbCl₂-modified perovskite ink.

Conclusion

In summary, this study establishes a viable blade-coating strategy under ambient conditions for fabricating high-quality perovskite films by employing strategic chloride additive engineering. We demonstrated that vacuum quenching, when combined with the right additive, can effectively control crystallization dynamics and suppress the non-radiative recombination in an air environment, eliminating the need for inert atmospheres. Our comparative investigation reveals that the site of chloride incorporation critically dictates the final film properties and device performance. The introduction of Cl⁻ at the X-site via PbCl₂ proved highly beneficial, as it moderately slowed crystallization and suppressed the non-radiative recombination, promoting the growth of large, highly crystalline grains. In contrast, the dual A-/X-site modification from Cl-PACl, while also slowing crystallization, introduced detrimental effects. The large organic cation (Cl-PA⁺) increased non-radiative recombination, ultimately degrading device performance. The superior material quality achieved with PbCl₂ modification directly translated to enhanced photovoltaic performance and operational stability, yielding a champion PSC efficiency of 24.2% and exceptional thermal-light stability. The



successful fabrication of a mini-module with 18.0% efficiency further validates the scalability and industrial promise of this PbCl_2 -assisted blade-coating process. This work provides critical insight into the role of additive incorporation mechanisms and offers a practical and effective pathway for the ambient-air manufacturing of efficient and stable perovskite photovoltaics.

Supporting Information

Experimental section; SEM; EDS; XPS; in-situ transmission; transient absorption spectroscopy; J-V curve of solar cells.

Acknowledgments

H. W. acknowledges the financial support by the Air Force Office of Scientific Research (AFOSR) under award number FA9550-17-1-0099 and FA9550-21-1-0192. This work was authored in part by the National Laboratory of the Rockies, for the U.S. Department of Energy (DOE) under Contract No. DE-AC36-08GO28308. The views expressed in the article do not necessarily represent the views of the DOE or the U.S. Government. F. Y., Y. W., and K. K. acknowledge the financial support by the National Science Foundation TI-2329871 and ECCS-2413632. L.W.-B. acknowledges support from the NSF under award number DMR 2326228. This work made use of University of Utah shared facilities of the Micron Technology Foundation Inc. Microscopy Suite sponsored by the John and Marcia Price College of Engineering, Health Sciences Center, Office of the Vice President for Research.

Author contributions

Z.C. and V.E.G. carried out the experiments, including perovskite film and device fabrication, device test, in-situ PL and transmission measurements, XRD, absorption, TRPL, and transient absorption spectroscopy. H.W. conceived and supervised the project and designed the experiments. Z.C. and H.W. wrote the manuscript. D.N.M., X.Z., and J.M.L. performed and analyzed the SEM measurements. Y.W., K.K., and F.Y. conducted the XPS measurements and data analysis. J.K.J., A.B., and L.W.-B. performed and analyzed the EDS measurements. All authors contributed to the discussion of the results, revised and edited the manuscript.



References:

View Article Online
DOI: 10.1039/D6TA01022A

1. NREL Best Research-Cell PV Efficiency Chart. <https://www.nrel.gov/pv/interactive-cell-efficiency> (accessed 12/30/2025).
2. Meng, L.; You, J.; Yang, Y., Addressing the stability issue of perovskite solar cells for commercial applications. *Nat. Commun.* **2018**, *9*, 5265.
3. Kim, J. Y.; Lee, J.-W.; Jung, H. S.; Shin, H.; Park, N.-G., High-efficiency perovskite solar cells. *Chem. Rev.* **2020**, *120*, 7867.
4. Green, M. A.; Ho-Baillie, A.; Snaith, H. J., The emergence of perovskite solar cells. *Nat. Photonics* **2014**, *8*, 506.
5. Correa-Baena, J.-P.; Saliba, M.; Buonassisi, T.; Grätzel, M.; Abate, A.; Tress, W.; Hagfeldt, A., Promises and challenges of perovskite solar cells. *Science* **2017**, *358*, 739.
6. Patidar, R.; Burkitt, D.; Hooper, K.; Richards, D.; Watson, T., Slot-die coating of perovskite solar cells: An overview. *Mater. Today Commun.* **2020**, *22*, 100808.
7. Deng, Y.; Peng, E.; Shao, Y.; Xiao, Z.; Dong, Q.; Huang, J., Scalable fabrication of efficient organolead trihalide perovskite solar cells with doctor-bladed active layers. *Energy Environ. Sci.* **2015**, *8*, 1544.
8. Deng, Y.; Dong, Q.; Bi, C.; Yuan, Y.; Huang, J., Air-Stable, Efficient Mixed-Cation Perovskite Solar Cells with Cu Electrode by Scalable Fabrication of Active Layer. *Adv. Energy Mater.* **2016**, *6*, 1600372.
9. Li, J.; Munir, R.; Fan, Y.; Niu, T.; Liu, Y.; Zhong, Y.; Yang, Z.; Tian, Y.; Liu, B.; Sun, J., Phase transition control for high-performance blade-coated perovskite solar cells. *Joule* **2018**, *2*, 1313.
10. Liu, J.; Zhang, M.; Sun, X.; Xiang, L.; Yang, X.; Hu, X.; Wang, Z.; Hou, T.; Qin, J.; Huang, Y., Scalable Fabrication of Methylammonium-Free Wide-Bandgap Perovskite Solar Cells by Blade Coating in Ambient Air. *Nano-Micro Lett.* **2025**, *17*, 318.
11. Cha, H.-C.; Huang, S.-H.; Li, C.-F.; Tsai, F.-Y.; Su, W.-F.; Huang, Y.-C., Advances and strategies in scalable coating techniques for flexible perovskite solar cells. *Sustain. Energy Fuels.* **2025**, *9*, 5962.
12. Leguy, A. M.; Hu, Y.; Campoy-Quiles, M.; Alonso, M. I.; Weber, O. J.; Azarhoosh, P.; Van Schilfgaarde, M.; Weller, M. T.; Bein, T.; Nelson, J., Reversible hydration of $\text{CH}_3\text{NH}_3\text{PbI}_3$ in films, single crystals, and solar cells. *Chem. Mater.* **2015**, *27*, 3397.
13. Wang, Q.; Chen, B.; Liu, Y.; Deng, Y.; Bai, Y.; Dong, Q.; Huang, J., Scaling behavior of moisture-induced grain degradation in polycrystalline hybrid perovskite thin films. *Energy Environ. Sci.* **2017**, *10*, 516.
14. Hidalgo, J.; Kaiser, W.; An, Y.; Li, R.; Oh, Z.; Castro-Méndez, A.-F.; LaFollette, D. K.; Kim, S.; Lai, B.; Breternitz, J., Synergistic role of water and oxygen leads to degradation in formamidinium-based halide perovskites. *J. Am. Chem. Soc.* **2023**, *145*, 24549.
15. Gu, L.; Fei, F.; Xu, Y.; Wang, S.; Yuan, N.; Ding, J., Vacuum quenching for large-area perovskite film deposition. *ACS Appl. Mater. Interfaces* **2022**, *14*, 2949.
16. Zhang, X.; Baral, P.; Chakraborty, N.; Garden, K.; Shen, L.; Vijayaraghavan, S. N.; Cao, Z.; Yan, F.; Gong, X.; Whittaker-Brooks, L.; Wang, H., Blade coating inverted perovskite solar



- cells with vacuum-assisted nucleation based on bottom quasi-2D passivation. *Solar RRL* **2023**, *7*, 2200900. View Article Online
DOI: 10.1039/D3JA01022A
17. Baral, P.; Zhang, X.; Garden, K.; Chakraborty, N.; Shen, L.; Cao, Z.; Gong, X.; Whittaker-Brooks, L.; Wang, H., Efficient and stable perovskite solar cells based on blade-coated $\text{CH}_3\text{NH}_3\text{PbI}_3$ thin films fabricated using “green” solvents under ambient conditions. *Org. Electron.* **2023**, *116*, 106763.
18. Zhang, X.; Cao, Z.; Shen, L.; Garden, K.; Chakraborty, N.; Baral, P.; Whittaker-Brooks, L.; Gong, X.; Luther, J. M.; Wang, H., Unraveling the Combined Photothermal Stability of Common Perovskite Solar Cell Compositions. *ACS Energy Lett.* **2024**, *9*, 5728.
19. Zhou, H.; Cai, K.; Yu, S.; Wang, Z.; Xiong, Z.; Chu, Z.; Chu, X.; Jiang, Q.; You, J., Efficient and stable perovskite mini-module via high-quality homogeneous perovskite crystallization and improved interconnect. *Nat. Commun.* **2024**, *15*, 6679.
20. Picart, C.; Khawaja, K. A.; Cao, Z.; Wang, Y.; Gu, X.; Wall, J.; Li, L.; Wang, H.; Yan, F., Cold air quench control of local crystallization environment in fully air-processed carbon-based perovskite solar cells. *Nano Energy* **2026**, *148*, 111647.
21. Li, L.; Chen, Y.; Liu, Z.; Chen, Q.; Wang, X.; Zhou, H., The Additive Coordination Effect on Hybrids Perovskite Crystallization and High-Performance Solar Cell. *Adv. Mater.* **2016**, *28*, 9862.
22. Ma, J.; Wang, L.; He, K.; Sun, Y.; Li, B.; Zhao, Q.; Du, B., Progress and challenges: a review of ionic liquid treatment for efficient and stable perovskite solar cells. *J. Mater. Chem. C* **2024**, *12*, 10837.
23. Lee, D.-K.; Park, N.-G., Additive engineering for highly efficient and stable perovskite solar cells. *Appl. Phys. Rev.* **2023**, *10*, 011308.
24. Li, T.; Pan, Y.; Wang, Z.; Xia, Y.; Chen, Y.; Huang, W., Additive engineering for highly efficient organic–inorganic halide perovskite solar cells: recent advances and perspectives. *J. Mater. Chem. A* **2017**, *5*, 12602.
25. Kim, M.; Kim, G.-H.; Lee, T. K.; Choi, I. W.; Choi, H. W.; Jo, Y.; Yoon, Y. J.; Kim, J. W.; Lee, J.; Huh, D., Methylammonium chloride induces intermediate phase stabilization for efficient perovskite solar cells. *Joule* **2019**, *3*, 2179.
26. Odysseas Kosmatos, K.; Theofylaktos, L.; Giannakaki, E.; Deligiannis, D.; Konstantakou, M.; Stergiopoulos, T., Methylammonium Chloride: A Key Additive for Highly Efficient, Stable, and Up-Scalable Perovskite Solar Cells. *Energy Environ. Mater.* **2019**, *2*, 79.
27. Shen, X.; Gallant, B. M.; Holzhey, P.; Smith, J. A.; Elmestekawy, K. A.; Yuan, Z.; Rathnayake, P.; Bernardi, S.; Dasgupta, A.; Kasparavicius, E., Chloride-Based Additive Engineering for Efficient and Stable Wide-Bandgap Perovskite Solar Cells. *Adv. Mater.* **2023**, *35*, 2211742.
28. Pham, N. D.; Tiong, V. T.; Chen, P.; Wang, L.; Wilson, G. J.; Bell, J.; Wang, H., Enhanced perovskite electronic properties via a modified lead (ii) chloride Lewis acid–base adduct and their effect in high-efficiency perovskite solar cells. *J. Mater. Chem. A* **2017**, *5*, 5195.
29. Li, B.; Zhang, Y.; Zhang, L.; Yin, L., PbCl_2 -tuned inorganic cubic CsPbBr_3 (Cl) perovskite solar cells with enhanced electron lifetime, diffusion length and photovoltaic performance. *J. Power Sources* **2017**, *360*, 11.



30. Stone, K. H.; Gold-Parker, A.; Pool, V. L.; Unger, E. L.; Bowring, A. R.; McGeehan, M. D.; Toney, M. F.; Tassone, C. J., Transformation from crystalline precursor to perovskite in PbCl₂-derived MAPbI₃. *Nat. Commun.* **2018**, *9*, 3458.
31. Zhang, Y.; Li, Y.; Zhang, L.; Hu, H.; Tang, Z.; Xu, B.; Park, N. G., Propylammonium chloride additive for efficient and stable FAPbI₃ perovskite solar cells. *Adv. Energy Mater.* **2021**, *11*, 2102538.
32. Muscarella, L. A.; Petrova, D.; Jorge Cervasio, R.; Farawar, A.; Lugier, O.; McLure, C.; Slaman, M. J.; Wang, J.; Ehrler, B.; Von Hauff, E., Air-stable and oriented mixed lead halide perovskite (FA/MA) by the one-step deposition method using zinc iodide and an alkylammonium additive. *ACS Appl. Mater. Interfaces* **2019**, *11*, 17555.
33. Sharma, B.; Garai, R.; Afroz, M. A.; Sharma, T.; Choudhary, S.; Singh, R. K.; Satapathi, S., Enhancing Light Utilization Efficiency of Semi-Transparent Perovskite Solar Cells via Tailored Interfacial Engineering. *Adv. Energy Mater.* **2024**, *14*, 2402473.
34. Liu, K.; Luo, Y.; Jin, Y.; Liu, T.; Liang, Y.; Yang, L.; Song, P.; Liu, Z.; Tian, C.; Xie, L., Moisture-triggered fast crystallization enables efficient and stable perovskite solar cells. *Nat. Commun.* **2022**, *13*, 4891.
35. Tan, W. L.; McNeill, C. R., X-ray diffraction of photovoltaic perovskites: Principles and applications. *Appl. Phys. Rev.* **2022**, *9*, 021310.
36. Roose, B.; Dey, K.; Chiang, Y.-H.; Friend, R. H.; Stranks, S. D., Critical assessment of the use of excess lead iodide in lead halide perovskite solar cells. *J. Phys. Chem. Lett.* **2020**, *11*, 6505.
37. Wang, M.; Fei, C.; Uddin, M. A.; Huang, J., Influence of voids on the thermal and light stability of perovskite solar cells. *Sci. Adv.* **2022**, *8*, eabo5977.
38. Yu, B.; Wei, X.; Yu, H., Crystallization Phase Transition and Buried Interface Modulate via Bifunctional Organic Ligands toward Efficient and Stable Inverted MA/Br-Free Perovskite Solar Cells. *Adv. Funct. Mater.* **2026**, *36*, e22445.
39. Zhang, Y.; Yu, H., Phase-controlled crystallization strategy for stable α -phase perovskite solar cells prepared in air. *Chem. Eng. J.* **2026**, *531*, 173913.
40. Herz, L. M., Charge-carrier dynamics in organic-inorganic metal halide perovskites. *Annu. Rev. Phys. Chem.* **2016**, *67*, 65.
41. Yang, G.; Tu, Y.; Ye, J.; Liu, R.; Zang, Y.; Zhang, L.; Wang, Y.; Li, G.; Zhou, Q.; Chu, L., Study on carrier dynamics of perovskite solar cells via transient absorption. *J. Alloy. Compd.* **2023**, *952*, 170051.
42. Srivastava, S.; Ranjan, S.; Yadav, L.; Sharma, T.; Choudhary, S.; Agarwal, D.; Singh, A.; Satapathi, S.; Gupta, R. K.; Garg, A., Advanced spectroscopic techniques for characterizing defects in perovskite solar cells. *Commun. Mater.* **2023**, *4*, 52.
43. Fei, C.; Li, N.; Wang, M.; Wang, X.; Gu, H.; Chen, B.; Zhang, Z.; Ni, Z.; Jiao, H.; Xu, W., Lead-chelating hole-transport layers for efficient and stable perovskite minimodules. *Science* **2023**, *380*, 823.
44. Fei, C.; Kuvayskaya, A.; Shi, X.; Wang, M.; Shi, Z.; Jiao, H.; Silverman, T. J.; Owen-Bellini, M.; Dong, Y.; Xian, Y., Strong-bonding hole-transport layers reduce ultraviolet degradation of perovskite solar cells. *Science* **2024**, *384*, 1126.



45. Silverman, T. J.; Repins, I. R., Diagonal shadows could cause arcs in thin-film modules with P4 scribes. *IEEE J. Photovolt.* **2023**, *13*, 917. [View Article Online](#)
DOI: 10.1093/ijl/dtad010



Data Availability Statement

The data supporting this article have been included as the Supplementary Information (SI).

